

Such results will be critical for assessing experimentally the nature of pinning by correlated defects, for testing (and guiding) theories that are being developed to understand these systems, and for devising methods for enhancing further critical currents in the high- T_c materials.

REFERENCES AND NOTES

1. D. J. Bishop, P. L. Gammel, D. A. Huse, C. A. Murray, *Science* **255**, 165 (1992).
2. D. A. Huse, M. P. A. Fisher, D. S. Fisher, *Nature* **358**, 553 (1992).
3. G. Taubes, *Science* **261**, 1521 (1993).
4. L. Civale *et al.*, *Phys. Rev. Lett.* **67**, 648 (1991).
5. R. C. Budhani, M. Suenaga, S. H. Liou, *ibid.* **69**, 3816 (1992).
6. W. Gerhauser *et al.*, *ibid.* **68**, 879 (1992).
7. Y. Zhu, Z. X. Cai, R. C. Budhani, M. Suenaga, D. O. Welch, *Phys. Rev. B* **48**, 6436 (1993).
8. Columnar defects also shift the apparent irreversibility line, which defines the boundary in the magnetic field-temperature plane between reversible and irreversible flux motion, upward in these materials.
9. D. R. Nelson and V. M. Vinokur, *Phys. Rev. Lett.* **68**, 2398 (1992); *Phys. Rev. B* **48**, 13060 (1993).
10. W. Jiang *et al.*, *Phys. Rev. Lett.* **72**, 550 (1994); R. C. Budhani, W. L. Holstein, M. Suenaga, *ibid.*, p. 566.
11. S. Behler *et al.*, *ibid.*, p. 1750.
12. H. Dai, J. Liu, C. M. Lieber, *ibid.*, p. 748.
13. D. S. Ginley *et al.*, *J. Mater. Res.* **9**, 1126 (1994).
14. AFM images acquired with the sample rotated at different angles while keeping the scan direction the same with respect to the tip demonstrated that the shape of the etch pits is intrinsic and does not reflect a convolution of the tip geometry. SEM and optical microscopy studies also support the inverted pyramid geometry assigned to the pits.
15. H. Dai and C. M. Lieber, *Annu. Rev. Phys. Chem.* **44**, 237 (1993).
16. J. P. Hansen and I. R. McDonald, *Theory of Simple Liquids* (Academic Press, New York, 1976).
17. D. R. Nelson, *Physica A* **177**, 220 (1991).
18. Images recorded in the regime where the areal defect density is greater than the flux-line density show that only some of the etch pits are decorated by magnetic particles (for example, Fig. 4A). These results show that it is not simply the presence of etch pits that attracts the particles; a flux line must also exist on the columnar defect site.
19. Because the same density of FLL topological defects is observed on unetched samples, we believe that the etch pits do not affect the overall FLL structure.
20. The orientational correlation function is defined as $G_6(\mathbf{r}) = \langle \psi_6^*(0) \psi_6(\mathbf{r}) \rangle$ where the orientational order parameter
$$\psi_6(\mathbf{r}) = \sum_{i=1}^n \exp[i6\theta_i(\mathbf{r})]/n$$
 is summed over all n nearest neighbors of a vortex at \mathbf{r} (15). For the samples containing columnar defects, the orientational correlation function can be fitted to an exponential,
$$G_6(r) \propto \exp(-r/\xi_6)$$
 where the correlation length, ξ_6 , equals the average defect spacing.
21. The same values of ξ_7 and ξ_6 were determined from analyses of Bitter patterns formed on unetched samples. These results quantitatively confirm that the etch pits do not affect the overall FLL structure.
22. M. Leghissa, L. A. Gurevich, M. Kraus, G. Saemannschiernko, L. Y. Vinnikov, *Phys. Rev. B* **48**, 1341 (1993).
23. The long-range interaction depends logarithmically on separation, $\ln(r/\lambda)$, and should become important when $a_0 \leq \lambda$, the magnetic penetration depth. This criterion seemingly is not met in our decoration experiments carried out at 4.2 K where $\lambda \approx 0.2 \mu\text{m} < a_0$. However, if the FLL structure is frozen at a higher temperature, the results are

understandable because λ diverges with temperature as

$$\lambda(T) \approx \lambda(0) [1 - (T/T_c)^4]^{-1/2}$$

in the two-fluid model. Using this expression to estimate the temperature where $a_0 \approx \lambda$ yields $T = 0.98 T_c$; this value is close to the apparent irreversibility temperature (at the corresponding field) for these samples.

24. U. Tauber, H. Dai, D. R. Nelson, C. M. Lieber, unpublished material.
25. We thank D. R. Nelson and U. Tauber for helpful discussions. C.M.L. acknowledges support by the National Science Foundation (grant DMR 9306684) and the Harvard Materials Research Laboratory.

20 May 1994; accepted 18 July 1994

Lattice Location of Trace Elements Within Minerals and at Their Surfaces with X-ray Standing Waves

Yonglin Qian, Neil C. Sturchio, Ronald P. Chiarello, Paul F. Lyman, Tien-Lin Lee, Michael J. Bedzyk*

The x-ray standing waves generated by dynamical Bragg diffraction were used to directly measure lattice locations of trace elements within and at the surface of a mineral single crystal. These high-precision measurements were made on natural Iceland spar calcite cleaved along the (10 $\bar{1}$ 4) plane and reacted with a dilute aqueous lead solution. Within the bulk crystal, naturally occurring trace manganese was found within (10 $\bar{1}$ 4) planes, consistent with its substitution for calcium. At the crystal surface, sorbed lead was found to be highly ordered and mostly within (10 $\bar{1}$ 4) planes. This demonstrates a powerful application of synchrotron radiation in the earth and environmental sciences.

Knowledge of the crystallographic locations of minor and trace elements within minerals and at their surfaces is important for a wide range of applications in the earth and environmental sciences. This knowledge facilitates a more rigorous understanding of dynamic natural processes (for example, the genesis of rocks and minerals, the transport of contaminants in ground waters, biomineralization, and the history of Earth's climate). The classical approach to determining sites of elements in minerals combines x-ray diffraction structure refinements with bulk chemical analyses and crystal-chemical reasoning. As a complement to this approach, a range of spectroscopic methods allowing improved solid-state characterization has gained widespread use during recent decades (1).

Atomic-scale processes at mineral surfaces have been receiving increased attention because of their importance in environmental geochemistry. This has been stimulated by the advent of new techniques and facilities, such as atomic force microscopy and high-brilliance synchrotron radiation sources, which allow unprecedented

studies of atomic-scale processes at mineral surfaces (2-5). This report demonstrates an additional technique involving the use of x-ray standing waves as an element-specific structural probe to directly provide precise (~0.04 Å) data on the crystallographic site locations of trace elements in minerals and at their surfaces.

On the basis of von Laue and Ewald's dynamical theory for x-ray diffraction (6), Batterman (7) demonstrated that an x-ray standing wave (XSW) is generated inside a perfect single crystal during Bragg diffraction. Later, Cowan, Golovchenko, and Robbins (8) showed that the XSW not only exists inside the crystal but also extends above the surface (Fig. 1). The length scale of the standing wave probe is characterized by its period, which is equal to the d spacing of the diffraction planes. Rocking the crystal in angle θ (or scanning the incident photon energy) through the Darwin curve of a strong Bragg reflection causes the antinodes of the standing wave to shift inward by one-half of a period. By monitoring the modulation of the fluorescence yield from a specific atomic species while phase-shifting the XSW, one can determine the atomic position (or distribution) relative to the bulk diffraction plane. Thus, the XSW method directly solves the "phase problem" inherent to conventional diffraction methods and has proven to be a highly precise probe for measurement of the positions of impurity atoms at the surface and within artificially grown perfect single crystals (7-11).

For this experiment, we used natural calcite (Fig. 1). The rhombohedral calcite

Y. Qian and M. J. Bedzyk, Materials Science Division, Argonne National Laboratory, Argonne, IL 60439, and Department of Materials Science and Engineering and Materials Research Center, Northwestern University, Evanston, IL 60208, USA.
N. C. Sturchio and R. P. Chiarello, Geoscience/CMT-205, Argonne National Laboratory, Argonne, IL 60439, USA.
P. F. Lyman and T.-L. Lee, Department of Materials Science and Engineering and Materials Research Center, Northwestern University, Evanston, IL 60208, USA.

*To whom correspondence should be addressed.

(CaCO₃) structure is conventionally described in terms of a hexagonal unit cell with alternating basal planes of Ca and CO₃. We investigated the distribution of naturally occurring trace Mn within calcite and artificially sorbed Pb at the (10 $\bar{1}$ 4) calcite cleavage surface with (10 $\bar{1}$ 4) XSW measurements ($d_{10\bar{1}4} = 3.036 \text{ \AA}$). We chose Pb for the sorption measurements because of its geochemical importance and because it did not appear as a bulk trace element and has a very strong α fluorescence signal.

The samples were cleaved from a large single, optically clear Iceland spar calcite crystal from Chihuahua, Mexico. After rinsing the crystals with distilled water, acetone, and methanol, we cleaved them along the (10 $\bar{1}$ 4) plane to obtain a pristine surface. The samples were 5 mm wide, 8 mm long, and 2 mm thick. Immediately after cleavage, some samples were reacted with a dilute (ground water-like) Na-Ca-HCO₃-Cl aqueous solution (ionic strength = 0.0038) containing Pb and ethylenediaminetetraacetate (EDTA) at respective concentrations of 10 and 15 μmol (12). The reactions of the samples with this Pb solution were conducted at room temperature with reaction times ranging from 5 min to 8 hours. Each reacted sample was then blown dry with a jet of nitrogen gas to remove solution remaining on the surface and was kept in a helium atmosphere throughout the x-ray measurement.

Our XSW experiments were performed at beam line X15A of the National Synchrotron Light Source (Fig. 2). We first measured an unreacted, cleaved calcite sample and then a series of samples that were reacted with the Pb solution. The incident photon energy from the Si(111) double-crystal monochromator was calibrated to be $E_\gamma = 13.8 \text{ keV}$ with a resolution width of $\Delta E = 1.0 \text{ eV}$. The incident slits for our two-circle diffractometer produced a beam 0.6 mm high and 2.2 mm wide. This gave an incident flux of 2.2×10^9 photons per second. We scanned the incident angle θ through the calcite (10 $\bar{1}$ 4) rocking curve and simultaneously recorded the Bragg-reflected intensities with a NaI detector and the fluorescence spectra with an energy dispersive Si(Li) detector (Fig. 2). The slits between the sample and the Si(Li) detector limited the fluorescence emission take-off angle α to $0^\circ < \alpha < 4.8^\circ$. It took 6 hours to collect the data containing both the calcite (10 $\bar{1}$ 4) reflectivity and the CaK α , MnK α , and PbL α fluorescence yields from the sample reacted for 8 hours (Fig. 3).

The experimental reflectivity curve (rocking curve) had a nearly ideal fit to the dynamical diffraction theory curve for a perfect single crystal (Fig. 3). This agreement between theory and experimental al-

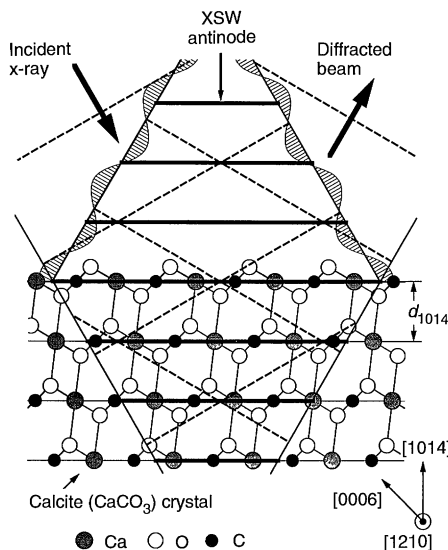


Fig. 1. A sketch of the XSW generated by Bragg diffraction from the calcite (10 $\bar{1}$ 4) diffraction planes. The diffraction plane spacing is $d_{10\bar{1}4} = 3.036 \text{ \AA}$. On the high-angle side of the rocking curve, antinodal planes of the XSW are aligned with (10 $\bar{1}$ 4) diffraction planes, as shown. On the low-angle side, nodes are aligned with (10 $\bar{1}$ 4) planes. The calcite structure is projected along the [1210] direction. Note that Ca, C, and one of the three O atoms (which projects at the C position) are centered on (10 $\bar{1}$ 4) planes.

lows us to apply quantitative XSW analysis to our fluorescence yields, which should vary as a function of angle θ according to the following parameterized equation (10)

$$Y(\theta) = Y_{\text{OB}} [1 + R + 2\sqrt{R} f_{c,H} \cos(\psi - 2\pi P_H)] Z(\theta) \quad (1)$$

where Y_{OB} is the off-Bragg fluorescence yield. The reflectivity $R(\theta)$, the XSW phase $\psi(\theta)$, and the effective thickness $Z(\theta)$ are derived from dynamical diffraction theory (13). The coherent fraction $f_{c,H}$ and the coherent position P_H represent the amplitude and phase of the H th Fourier component of the spatial distribution of the fluorescent atomic species. The coherent position is a $\Delta d/d$ position ranging from 0 to 1, where 0 and 1 correspond to the diffraction planes and 0.5 corresponds to a position halfway between the diffraction planes. The coherent fraction, which also ranges from 0 to 1, measures the spread of the atom distribution. By a χ^2 fit of Eq. 1 to the data in Fig. 3, we obtained the parameters Y_{OB} , $f_{c,10\bar{1}4}$, and $P_{10\bar{1}4}$ for Ca, Mn, and Pb (Table 1).

Our measured value of $P_{10\bar{1}4}$ for Ca shows that it is located precisely ($\pm 0.03 \text{ \AA}$) in (10 $\bar{1}$ 4) diffraction planes, as expected (Fig. 1). This excellent consistency gives convincing proof for the validity of our technique as applied to natural calcite. The

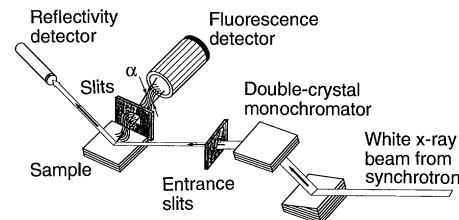


Fig. 2. Experimental setup for XSW measurements. The 6° asymmetric cut of the first Si(111) monochromator crystal serves to optically collimate the emission from the monochromator.

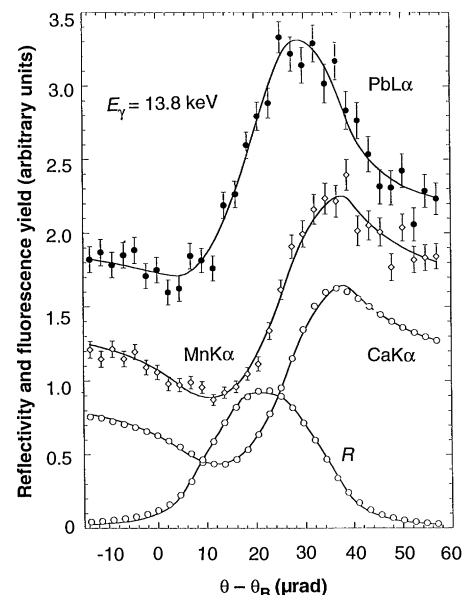


Fig. 3. Experimental data and theory curves for calcite (10 $\bar{1}$ 4) reflectivity and normalized fluorescence yields of CaK α , MnK α , and PbL α from calcite reacted with Pb solution for 8 hours. For the purpose of clarity, Mn and Pb curves are offset by 0.5 and 1, respectively. The theory curves have been convoluted by the 10- μrad -wide emittance function from the Si(111) monochromator-collimator. Although Ca, Mn, and Pb all lie on (10 $\bar{1}$ 4) planes according to the analysis, the Ca and Mn yields appear to have a slightly different phase than the Pb yield because of the extinction effect (13).

measured value of $P_{10\bar{1}4}$ for Mn also shows that Mn lies precisely in (10 $\bar{1}$ 4) planes, implying that Mn²⁺ occupies Ca²⁺ sites. On the basis of our measured off-Bragg fluorescence yields (Table 1) and tabulated values for photoeffect cross sections (14), fluorescence yields (15), and calcite absorption coefficients for the Ca and Mn outgoing photons, we estimate that the fraction of Ca sites occupied by Mn is 400 parts per million (ppm) for this sample. This value was approximately identical for each of our samples.

The values of $f_{c,10\bar{1}4}$ for Ca and Mn (Table 1) should be equal to the product of the Debye-Waller factor, which accounts

Table 1. The energies E_{out} and linear absorption coefficients μ_{out} in CaCl_2 for outgoing fluorescence x-rays. The XSW-measured parameters for the calcite (1014) reflection are off-Bragg fluorescence yield Y_{OB} (in counts per second), coherent position $P_{10\bar{1}4}$, and coherent fraction $f_{c, 10\bar{1}4}$.

	E_{out} (keV)	μ_{out} (cm^{-1})	Y_{OB} (cps)	$P_{10\bar{1}4}$	$f_{c, 10\bar{1}4}$
CaK α	3.69	314	4063	0.01 ± 0.01	0.85 ± 0.01
MnK α	5.90	461	5.44	0.00 ± 0.01	0.94 ± 0.02
PbL α	10.55		1.31	0.00 ± 0.01	0.66 ± 0.03

for thermal vibration, and the static Debye-Waller factor, which accounts for crystalline defects and disorder. The fact that values of $f_{c,10\bar{1}4}$ for Ca and Mn approach unity is consistent with the near-ideal experimental rocking curve of the calcite.

The PbL α fluorescence signal was below our limit of detection for calcite reacted with the Pb solution for 4 hours or less. For calcite reacted for 8 hours with the Pb solution, we found a detectable PbL α fluorescence that corresponded to a coverage of $\Theta_{Pb} = 0.08$ monolayer (ML) based on a fluorescence yield analysis. For this sample, we found that the Pb coherent fraction was 0.66, and the Pb coherent position was 0.00. The simplest explanation for these measured values is that 66% of the Pb atoms (0.05 ML) occupy positions within a (10 $\bar{1}$ 4) diffraction plane. This ordered fraction of 66% is a high value for a "real" surface that has been exposed to laboratory atmosphere. The incoherent fraction of 0.34 corresponds primarily to randomly distributed Pb, which could include physisorbed hydrated Pb ions, Pb chemisorbed at surface defect sites, multinuclear Pb complexes, and Pb affected by surface contamination. These data do not directly resolve the question of which (10 $\bar{1}$ 4) diffraction plane (or planes) the ordered Pb occupies. In the following discussion, we consider three possible structures for this ordered Pb: (i) a homoepitaxial calcite layer with trace Pb in solid solution, (ii) substitution of Pb for Ca within the calcite surface atom layer, and (iii) a Pb adlayer above the calcite surface atom layer.

To our knowledge, little information exists for the sorption of Pb on calcite; however, the behavior of Pb during this experiment may be compared with the recently studied sorption behavior of Sr and Ba on calcite (16); all are divalent ions and have similar ionic radii (Sr, 1.18 Å; Pb, 1.20 Å; and Ba, 1.35 Å) that are larger than that of Ca^{2+} (1.00 Å). Both Sr and Ba sorb weakly to the calcite surface from aqueous solution (log K value of surface exchange reaction near -2). Measured solid-liquid distribution coefficients for Sr and Ba coprecipitated with calcite are near 0.1 (17); as these depend on ionic radius, a similar value is expected

for Pb. If the ordered Pb was incorporated in a homoepitaxial Pb-bearing calcite layer, then the required thickness of this layer can be estimated. With the computed $\text{Pb}^{2+}/\text{Ca}^{2+}$ activity ratio in the experimental solution ($10^{-7.05}$) and the assumption that the solid-liquid distribution coefficient for Pb is that for Sr and Ba, such a layer would have to be almost 2 mm thick to contain the ordered Pb (0.05 ML equivalent). Because the data (Fig. 3) do not exhibit an extinction effect (13), the Pb must occur within a layer that is much thinner than the 7000 Å extinction depth. Thus, we can eliminate the homoepitaxial calcite layer as a possible structure for the sorbed Pb and conclude that the ordered Pb substitutes for Ca in the calcite surface atom layer or is present as an adlayer located by coincidence exactly one 3.04 \AA d spacing above the calcite surface atom layer. Although the relatively large ionic radius of Pb^{2+} makes it incompatible with the calcite structure (18), it may be reasonable to assume that at this low-coverage Pb could substitute for 5% of the surface Ca with localized strain. This issue can be better resolved by characterizing in-plane structure using off-specular XSW measurements (9).

The XSW measurements reported here demonstrate a high-resolution technique for element-specific, atomic-scale structural studies of trace elements within minerals and at their surfaces. This technique, which determines locations of trace elements to within 0.02 \AA relative to the bulk crystal lattice, can also be used for in situ liquid-solid interface studies (8, 19). The only comparable technique is x-ray absorption fine structure spectroscopy, which yields complementary information on short-range atomic order (1, 2). With the use of presently available synchrotron facilities, the sensitivity of the XSW technique ranges from 10^{12} to 10^{14} atoms per square centimeter for surface species to as low as 10 ppm for bulk impurities, depending on the sample and beamline characteristics. With the advent of much brighter x-ray sources such as the Advanced Photon Source, along with improvements in x-ray optics and fluorescence detectors, we anticipate significant increases in the sensitivity of the XSW

technique and its versatility to address fundamental problems in the earth and environmental sciences.

REFERENCES AND NOTES

1. F. C. Hawthorne, Ed., *Spectroscopic Methods in Mineralogy and Geology*, vol. 18 of *Reviews in Mineralogy* (Mineralogical Society of America, Washington, DC, 1988).
2. K. F. Hayes *et al.*, *Science* **238**, 783 (1987).
3. F. Ohnesorge and G. Binnig, *ibid.* **260**, 1451 (1993).
4. A. J. Gratz, P. E. Hillner, P. K. Hansma, *Geochim. Cosmochim. Acta* **57**, 491 (1993).
5. R. P. Chiarello, R. A. Wogelius, N. C. Sturchio, *ibid.* **57**, 4103 (1993).
6. For a review, see B. W. Batterman and H. Cole, *Rev. Mod. Phys.* **36**, 681 (1964).
7. B. W. Batterman, *Phys. Rev. A* **133**, 759 (1964); *Phys. Rev. Lett.* **22**, 703 (1969).
8. P. L. Cowan, J. A. Golovchenko, M. F. Robbins, *Phys. Rev. Lett.* **44**, 1680 (1980).
9. J. A. Golovchenko *et al.*, *ibid.* **49**, 560 (1982).
10. M. J. Bedzyk and G. Materlik, *Surf. Sci.* **152**, 10 (1985).
11. For a review on XSW measurements, see J. Zegenhagen, *Surf. Sci. Rep.* **18**, 199 (1993).
12. The addition of EDTA in excess of Pb has the effect of buffering $\text{Pb}^{2+}(\text{aq})$ at a constant value well below saturation of crystalline Pb phases [J. A. Davis, C. C. Fuller, A. D. Cook, *Geochim. Cosmochim. Acta* **51**, 1477 (1987)]. Before the addition of Pb and EDTA, the solution was reacted with calcite powder (grain size, 90 to 125 μm) in contact with atmosphere (partial pressure of CO_2 , $10^{-3.5}$ atm) for over 2 months. This allowed the solution to approach saturation with calcite and minimized the potential for reaction (other than Pb sorption) between the calcite surface and the experimental solution. The calcite was filtered out of the solution before addition of Pb and EDTA. The pH of the experimental solution was 8.15. The computed activity of aqueous Pb^{2+} was $10^{-10.3}$ and that of PbOH^+ was $10^{-8.85}$.
13. The normalized effective thickness $Z(\theta)$ is a constant, equal to unity if the fluorescent atoms are at the surface or within a depth z that is much less than the extinction depth [which is 7000 Å for the calcite (10 $\bar{1}$ 4) reflection]. If the atoms are uniformly distributed throughout the bulk crystal, then $Z(\theta) = [\mu_z(\text{OB}) + \mu_{out}\text{csc}\alpha] / [\mu_z(\theta) + \mu_{out}\text{csc}\alpha]$ (10), where $\mu_z(\theta)$ is the effective linear absorption coefficient for primary x-rays (7) and μ_{out} is the linear absorption coefficient for outgoing fluorescence. The extinction effect causes the penetration depth of primary x-rays, μ_z^{-1} , to change dramatically from 35 μm (off-Bragg) to 0.7 μm (on-Bragg). Thus, for Ca and Mn bulk atoms, the extinction effect would have obscured the interference effect in Eq. 1 if we had not reduced the average fluorescence emission take-off angle $\bar{\alpha}$ to 3.5° to make $(\sin \bar{\alpha})/\mu_{out}$ comparable to the extinction depth. The respective μ_{out} values are listed in Table 1.
14. D. T. Cromer, *J. Appl. Cryst.* **16**, 437 (1983).
15. M. O. Krause, *J. Phys. Chem. Ref. Data* **8**, 307 (1979).
16. J. M. Zachara, C. E. Cowan, R. T. Resch, *Geochim. Cosmochim. Acta* **55**, 1549 (1991).
17. N. E. Pingitore and M. P. Eastman, *ibid.* **50**, 2195 (1986).
18. R. J. Reeder, *Rev. Mineral.* **11**, 1 (1983).
19. M. J. Bedzyk, G. M. Bommarito, M. Caffrey, T. L. Penner, *Science* **248**, 52 (1990).
20. We acknowledge M. Beno and G. Knapp for helpful discussions. This work was supported by the Office of Basic Energy Sciences, U.S. Department of Energy, under contract W-31-109-ENG-38 to Argonne National Laboratory and contract DE-AC02-76CH00016 to National Synchrotron Light Source at Brookhaven National Laboratory and by the National Science Foundation under contract DMR-9120521 to the Materials Research Center at Northwestern University. P.F.L. is partially supported by National Institutes of Health under award IR01KD45295-01.

19 May 1994; accepted 19 July 1994